Core-shell structured $LiFePO_4$/C nanocomposite battery material for lithium production from brines

Min Zhang , Nuria Garcia-Araez

PII: S0013-4686(24)00926-5
DOI: https://doi.org/10.1016/j.electacta.2024.144686
Reference: EA 144686

To appear in: *Electrochimica Acta*

Received date: 5 January 2024
Revised date: 4 July 2024
Accepted date: 6 July 2024

Please cite this article as: Min Zhang , Nuria Garcia-Araez , Core-shell structured $LiFePO_4$/C nanocomposite battery material for lithium production from brines, *Electrochimica Acta* (2024), doi: https://doi.org/10.1016/j.electacta.2024.144686

Highlights

- -First application of core-shell battery materials for lithium production applications
- -Demonstration that the material properties requirements of $LiFePO_4$ for non-aqueous battery applications and for lithium production from brines are markedly different
- -Demonstration of the improved performance of core-shell carbon-coated $LiFePO_4$ materials over commercial materials for lithium production applications

Core-shell structured $LiFePO_4$/C nanocomposite battery material for lithium production from brines

Min Zhang [a*] *and Nuria Garcia-Araez* [ab*]

[a] School of Chemistry, University of Southampton, Highfield, Southampton SO17 1BJ, UK

[b] The Faraday Institution, Quad One, Harwell Campus, Didcot OX11 0RA, UK

* Corresponding authors: M.Zhang@soton.ac.uk (Min Zhang), N.Garcia-Araez@soton.ac.uk (Nuria Garcia-Araez)

Abstract

The development of affordable and environmentally friendly methods to produce lithium is urgently required to cope with the accelerating growth of the lithium battery market. Battery materials such as $LiFePO_4$ can be used to selectively sequestrate lithium from brine natural resources, thus producing a high-purity lithium salt for battery manufacture, but the long-term stability of the material is currently not sufficient for practical applications. Here, we report, for the first time, the development of a nanosized core-shell structured $LiFePO_4$/C material for applications in lithium production from brines. This $LiFePO_4$/C with a $LiFePO_4$-core (~123 nm size) covered by a pinhole-free carbon shell (~5 nm thickness) was prepared via solvothermal synthesis, and the carbon content was optimised to 5 wt%. The optimal core-shell structured $LiFePO_4$/C material exhibits a lithium extraction capacity of ca. 160 mA h g^{-1} at C/10 and ca. 130 mA h g^{-1} at 1C, and >87% capacity retention after 50 cycles of lithium sequestration and release at C/10 in synthetic brines. This excellent electrochemical performance is attributed to the homogenous nanosizing of the $LiFePO_4$ particles as well as the full coverage of the carbon coating, which provides effective protection by preventing the

direct contact of $LiFePO_4$ with the brines, thus stopping the surface degradation reactions that compromise the long-term stability. A direct comparison with three commercial $LiFePO_4$ materials demonstrates that, while similar performance is obtained in non-aqueous lithium-ion batteries, for lithium production applications, core-shell nanostructuring is crucial to achieve high capacity and preserve the material's longevity.

Keywords: lithium production, electrochemical lithium sequestration, brines, core-shell nanostructuring, lithium iron phosphate.

1. Introduction

Lithium-ion batteries have been widely used in portable devices such as laptops, smartphones and cameras, as well as in large-scale applications like electric vehicles, due to their high energy density, high power density and light weight.[1-3] The market demand for lithium is growing, while the future cost and availability of lithium are under debate.[4] Global resources of lithium are mainly in brines (which are concentrated saline solutions) and minerals. The lithium brines resources are about twice the size of the minerals, and the cost of lithium production from minerals is approximately double of that from brines.[5, 6] Over 45% of lithium resources are in the brines of Chile, Bolivia and Argentina, which contain cations such as sodium, potassium and magnesium in vast excess, compared to lithium, and thus the main challenge is to separate lithium from all other cations.[7, 8]

The current method of lithium production from brines is the lime-soda evaporation process, which is, unfortunately, very slow, water-consuming, waste-producing and weather-dependent.[9] Thus, there is a pressing need for the development of alternative, fast, cost-effective and environmentally friendly technologies for lithium production.[10] Several methods of lithium production from brines have been explored, such as chemical precipitation, ion-sieve adsorption, membrane technology, etc.[5, 11-13] A particularly

promising method is the electrochemical production of lithium using battery materials such as $LiMn_2O_4$/λ-MnO_2 and $LiFePO_4$/$FePO_4$.[10, 14-22] In this approach, lithium ions in the brine are extracted by a host battery material, then they are released in a recovery solution, during which the pristine host battery material is also recovered, thus making the whole process fully sustainable.[14, 23-27] Via this process, a highly pure lithium salt can be precipitated from the recovery solution. For practical applications, this electrochemical lithium production from brines requires the host battery materials to maintain high lithium absorption capacity and stability over long-term cycling, but this has not been achieved.[14, 28-30]

In order to understand the causes of capacity limitations and the long-term material degradation, we have used a nearly symmetrical cell design that contained two electrodes made with the same battery material but at different states of lithiation; specifically, we used a cell with a $LiFePO_4$ working electrode and a $Li_{0.25}FePO_4$ counter/reference electrode.[14] Using a commercial $LiFePO_4$ material, we demonstrated that the interfacial reactions of $LiFePO_4$ particles with the brines produced particle cracking and degradation of the lithium sequestration capacity with cycling.[14]

In this work, we have developed a novel nanosized core-shell structured $LiFePO_4$/C with a $LiFePO_4$-core covered by a pinhole-free carbon shell designed to prevent the detrimental interfacial reactions of $LiFePO_4$ in the brines. These core-shell structured $LiFePO_4$/C nanocomposites are compared with the commercial $LiFePO_4$/C to systematically investigate their lithium selectivity and cycling stability in the lithium production from brines. Three artificial brines representative of typical natural brines in Atacama (Chile), Olaroz (Argentina) and Central Altiplano (Bolivia), as well as a benchmark 0.5 M Li_2SO_4 solution, have been investigated. This is the first time that a core-shell structured $LiFePO_4$/C nanocomposite has been used for the electrochemical lithium production from brines. Also, this is the first

systematic study of the effect of the particle size and carbon coating of $LiFePO_4$/C for applications in lithium sequestration from brines.

2. Experimental

2.1. Materials synthesis

Six kinds of $LiFePO_4$/C samples were investigated, including three kinds of commercial $LiFePO_4$/C samples, i.e., LFP/C-1 (MTI Corporation), LFP/C-2 (Li-FUN Technology) and LFP/C-3 (Tatung Company), and three kinds of self-made core-shell nanostructured $LiFePO_4$/C samples, i.e., LFP/C-4, LFP/C-5 and LFP/C-6, as listed in Table 1.

The core-shell structured $LiFePO_4$/C samples were prepared via a solvothermal synthesis. Full details of the synthesis procedure are reported below, but briefly, a surfactant and chelating agent was used to form micelles in the solvothermal process, and a $LiFePO_4$ precursor was grasped inside the micelles due to the chelation effect.[31] In the following heat treatment, the micelles with carbon source surrounding the $LiFePO_4$ precursor became carbon-shell, and the precursor turned to $LiFePO_4$-core of the core-shell structure.[31]

The full synthesis procedure is as follows. The surfactant hexadecyltrimethylammonium bromide (CTAB, 0.246 mmol, ≥99% purity, Sigma Aldrich) was dispersed in deionised water first. Then, $LiOH•H_2O$ (0.0225 mol, ≥98% purity, Sigma Aldrich) and H_3PO_4 (0.0075 mol, 85 wt% assay, Sigma Aldrich) were added and stirred to form a white colloid. Subsequently, Na_2CO_3 (0.014 mmol, ≥99% purity, Sigma Aldrich) was mixed and stirred with appropriate amounts of carbon sources, i.e., formaldehyde (~1 mol, 36.5-38 wt% assay, Sigma Aldrich) and resorcinol (~1 mmol, ≥99% purity, Sigma Aldrich), then added to the white colloid with constant stirring to form a white suspension. After that, ascorbic acid ($C_6H_8O_6$, 0.475 mmol, 99% purity, Thermo Scientific) and $FeSO_4•7H_2O$ (0.0075 mol, ≥99% purity, Sigma Aldrich)

were dissolved in deionised water, and added to the white suspension with constant stirring to form a light green suspension. The suspension was heated in a Teflon-lined autoclave at 180 °C for 10 h. The precipitate was then washed with deionized water and dried at 80 °C for ≥5 h under a vacuum. The resulting material was heated at 3.5 °C min^{-1} to 650 °C for 4 h under a 5% H_2/Ar atmosphere to obtain $LiFePO_4$/C product.

For each of the six kinds of $LiFePO_4$/C samples here studied, the corresponding delithiated $FePO_4$/C samples were also prepared, and for that, a chemical delithiation procedure was followed,[32] and the obtained samples are denoted as FP/C-1, FP/C-2, FP/C-3, FP/C-4, FP/C-5 and FP/C-6, as listed in Table S1. For the chemical delithiation, $LiFePO_4$/C and $K_2S_2O_8$ (≥99% purity, Sigma Aldrich) with a molar ratio of 2:1 were mixed in ultrapure water (Purite, 18.2 MΩ cm) and stirred for 24 h at room temperature. The resulting material was filtered, washed with ultrapure water, and dried at 80 °C under a vacuum overnight. The resultant powder was ground and further dried at 120 °C under a vacuum for 3 days to obtain the $FePO_4$/C product.

2.2. Materials characterisation, batteries fabrication and electrochemistry

X-ray diffraction (XRD) used a Bruker D2 Phaser with Cu-K_α radiation. Rietveld fits to the XRD patterns were carried out using the GSAS package.[33] The crystallite sizes were calculated from the Lorentzian crystallite size broadening coefficient refined in the Rietveld fits to the XRD patterns, according to $\mathbf{p} = \frac{\mathbf{18000K\lambda}}{\mathbf{\pi L_x}}$, where p is the crystallite size (unit: nm), L_x is the refined crystallite size broadening value, K is the Scherrer constant, and λ is the wavelength of the incident X-rays (unit: nm).[33] Thermogravimetric analysis (TGA) was carried out using a Netzsch TG 209 F1 Libra with samples heated at 10 °C min^{-1} from 25 to 700 °C under an O_2 atmosphere. Scanning electron microscopy (SEM) was carried out using a JEOL JSM-6500F operated at 15 kV, and images were analysed using the ImageJ software.

Transmission electron microscopy (TEM) was carried out using a Hitachi HT7700 (120 kV). Raman spectroscopy used a Renishaw inVia confocal microscope, and the data were processed using the WiRE 4.1 software.

In addition, for the characterization of the lithium sequestration and release properties of the $LiFePO_4$/C materials in brines, electrochemical measurements were conducted using $LiFePO_4$ working electrodes, made with the $LiFePO_4$/C materials, cycled against $Li_{0.25}FePO_4$ counter/reference electrodes. The $LiFePO_4$ electrodes were prepared with $LiFePO_4$/C samples as the active material, whereas the $Li_{0.25}FePO_4$ electrodes were prepared with a mixture of $LiFePO_4$/C and the corresponding delithiated $FePO_4$/C samples in a mass ratio of 1:3 as the active material. $LiFePO_4$ and $Li_{0.25}FePO_4$ electrodes were fabricated by mixing the active material, carbon black (Super C65, Timcal) and polyvinylidene difluoride (PVDF 5130, Solvay) with a mass ratio of 8: 1: 1 in N-methyl-2-pyrrolidone (NMP, anhydrous, ≥99.8% purity, Sigma Aldrich). The slurry was cast onto a titanium foil (25 µm thickness, ≥99.6% purity, Advent Research Materials) with a wet thickness of 200 or 400 µm for $LiFePO_4$ and $Li_{0.25}FePO_4$ electrodes, respectively, and dried at 80°C under vacuum overnight. The coated foil was punched into circular discs with a diameter of 11 mm and pressed at 2 or ½ tons to obtain $LiFePO_4$ and $Li_{0.25}FePO_4$ electrodes, respectively. The active material mass loading was ≈ 2.5 mg cm^{-2} for $LiFePO_4$ and 5-6 mg cm^{-2} for $Li_{0.25}FePO_4$. The mass loadings of all the materials here studied were the same, thus enabling a reliable comparison.

Electrochemical extraction of lithium was performed in three different artificial brines, which represent typical compositions in the lithium reserves in Atacama (Chile),[25] Olaroz (Argentina),[34] and Central Altiplano (Bolivia),[35] as shown in Table 2. Note that higher salt concentrations have been reported for the Atacama brine in other studies,[36, 37] which correspond to the regions of the Salar that are under commercial exploitation.[38] The

artificial brines were prepared in air using ultrapure water and LiCl, NaCl, KCl and $MgCl_2•6H_2O$ (≥99% purity, Sigma Aldrich), whereas $Li_2SO_4•H_2O$ (≥99% purity, Sigma Aldrich) was used to prepare the benchmark Li_2SO_4 aqueous electrolyte. Although the presence of dissolved oxygen, from air, in the brines has been shown to accelerate the degradation of $LiFePO_4$ materials,[30] no attempt was made to remove it since that would be difficult to implement under practical applications.

The electrochemical measurements were done with ½ inch inner diameter Swagelok cells made of PFA (perfluoroalkoxy plastic with high chemical resistance), and with titanium bars as current collectors, since titanium is highly stable against corrosion in brines.[39] The cells were assembled in air with a $LiFePO_4$ working electrode, a $Li_{0.25}FePO_4$ counter/reference electrode and two glass fibre separators (GF/F grade, Whatman) with 150 µl of the artificial brines or aqueous Li_2SO_4 solution. The cells were left to rest for 10 h before the electrochemical tests. For the study of the electrochemical performance of $LiFePO_4$ electrodes in lithium half-cells, the cells were assembled in an argon-filled glovebox (MBraun, <1 ppm O_2, <1 ppm H_2O) with a standard organic electrolyte (LP57, 1 M $LiPF_6$ in EC:EMC 3:7 v/v, Soulbrain, 150 µl), and all cell parts were dried prior to cell assembly as described elsewhere.[40] Galvanostatic cycling tests were carried out using a Biologic potentiostat at charge/discharge rates of C/10 and 1C (e.g. a C-rate of C/10 for a theoretical specific capacity of 170 mA h g^{-1} corresponds to a specific current of 17 mA g^{-1}) within the potential range of -0.3 to 0.3 V (*vs.* $Li_{0.25}FePO_4$) and 2.5 to 4.1 V (*vs.* Li^+/Li).

3. Results and discussion

3.1. Characterisation of commercial $LiFePO_4$/C materials

Three kinds of commercial $LiFePO_4$/C materials (labelled LFP/C-1, LFP/C-2 and LFP/C-3) were investigated as host materials for the sequestration of lithium from brines. The crystallite and particle sizes and carbon content are summarized in Table 1.

The crystalline properties of the samples were investigated by XRD. Figure 1a shows that all the XRD peaks can be indexed to the standard olivine $LiFePO_4$ structure (PDF#83-2092 $LiFePO_4$, space group *Pnma*), as expected. The carbon coating on battery materials is typically amorphous, and, thus, it is not visible in the XRD pattern.[41] Fig. S1 shows the Rietveld fits to the XRD patterns, and the obtained lattice parameters (*a*, *b* and *c*), crystallite size broadening term (L_x) and reliability factors (R_{wp}, R_p) are listed in Table S2. These are typical $LiFePO_4$ lattice parameters, which are very close to the literature values.[31, 42, 43] The crystallite sizes (Table 1) calculated from the size-strain analysis during the Rietveld fits to the XRD patterns are 180, 181 and 173 nm for LFP/C-1, LFP/C-2 and LFP/C-3, respectively.

The morphology and particle size distribution of the samples was characterized by SEM, using the ImageJ software for particle size analysis, and the results are shown in Figure 1c. As summarized in Table 1, LFP/C-1 and LFP/C-2 show average particle sizes of ca. 630 and 620 nm, respectively, with very wide particle size distributions, whilst LFP/C-3 exhibits a larger average particle size of 790 nm and a slightly narrower, but still wide, particle size distribution.

The carbon contents in the $LiFePO_4$/C samples were estimated by TGA experiments. As shown in Figure 1b, the total mass changes were 3.0 wt%, 2.8 wt% and 2.7 wt% for LFP/C-1,

LFP/C-2 and LFP/C-3, respectively. Previous studies have shown that the mass changes in the TGA experiments are due to the oxidation of $LiFePO_4$ to $Li_3Fe_2(PO_4)_3$ and Fe_2O_3, leading to a mass gain, coupled with the burning of carbon into CO_2 gas, which produces a mass loss.[44, 45] The overall reaction is as follows:

$$\boldsymbol{LiFePO_4 + \frac{1}{4}O_2 + xC + xO_2 \rightarrow \frac{1}{3}Li_3Fe_2(PO_4)_3 + \frac{1}{6}Fe_2O_3 + xCO_2},$$

where *x* denotes the molar carbon content in the $LiFePO_4$/C sample. Using the reaction above, the carbon contents are calculated to be 2.0 wt%, 2.1 wt% and 2.3 wt% for LFP/C-1, LFP/C-2 and LFP/C-3, respectively, as listed in Table 1. The TEM images of the $LiFePO_4$/C samples (Figure 1d) show that the carbon coating is not complete and that it is unevenly distributed around the $LiFePO_4$ particles.

As will be shown below, for the study of the electrochemical performance of the $LiFePO_4$/C materials for the application in lithium production from brines, the experiments employed the delithiated form of $LiFePO_4$/C, here called $FePO_4$/C and labelled FP/C-1, FP/C-2 and FP/C-3. Fig. S2a shows that all the XRD peaks of the $FePO_4$/C samples can be indexed to the standard heterosite $FePO_4$ structure (PDF#34-0134 $FePO_4$, space group *Pnma*), meaning that the $FePO_4$ framework in the $LiFePO_4$ olivine structure is preserved.[43] The SEM images of the $FePO_4$/C samples (Fig. S2c) show that the morphology of $FePO_4$/C is not affected by the chemical delithiation process. The carbon contents in the $FePO_4$/C samples were estimated by TGA experiments, and the results are shown in Fig. S2b. The total mass changes were -2.1 wt%, -2.2 wt% and -2.4 wt% for FP/C-1, FP/C-2 and FP/C-3, respectively. The mass loss of $FePO_4$/C is attributed to the burning of carbon into CO_2 gas, since $FePO_4$ remains stable upon heating.[43] Thus, the carbon contents are determined to be 2.1 wt%, 2.2 wt% and 2.4 wt% for FP/C-1, FP/C-2 and FP/C-3, respectively, as listed in Table S1, in good agreement with the carbon content of the parental $LiFePO_4$/C samples, listed in Table 1. The TEM images of

$FePO_4$/C samples (Fig. S2d) show that the carbon coverage is partial and uneven, as in the parental $LiFePO_4$/C samples.

3.2. Electrochemical performance of commercial $LiFePO_4$/C materials

The electrochemical properties of the $LiFePO_4$/C materials were first assessed by galvanostatic cycling in lithium half-cells, using a standard organic battery electrolyte (LP57) and a standard, ink-based method of battery electrode preparation (see Experimental section). Fig. S3 shows the 1st and 2nd cycle charge/discharge profiles at a C-rate of C/10, from which it is concluded that all the materials deliver high specific capacities of ca. 160 mA h g^{-1}, thus confirming that all these commercial samples meet the requirements for non-aqueous lithium-ion battery applications. However, as we will show below, these commercial materials exhibit issues for applications in lithium production from brines.

For the evaluation of the performance of $LiFePO_4$/C materials in lithium production applications, the $LiFePO_4$/C battery electrodes were cycled in cells containing a $Li_{0.25}FePO_4$/C counter-and-reference electrode, as reported previously.[14] The reactions induced during cycling are the following:

$LiFePO_4 \rightleftharpoons FePO_4 + Li^+ + e^-$ at the working electrode

$2Li_{0.25}FePO_4 + Li^+ + e^- \rightleftharpoons 2Li_{0.75}FePO_4$ at the counter-and-reference electrode

The $Li_{0.25}FePO_4$/C electrode was prepared with a mixture of $LiFePO_4$/C and the corresponding delithiated $FePO_4$/C in a mass ratio of 1:3 as the active material, as described in the Experimental section. The electrolytes employed here are the benchmark Li_2SO_4 aqueous solution and artificial brines with compositions mimicking typical natural brines (Atacama, Olaroz and Central Altiplano) present in Chile, Argentina and Bolivia, respectively, where the latter contain sodium, potassium and magnesium in much higher concentrations

than lithium (Table 2). The 0.5 M Li_2SO_4 solution was employed as benchmark because it enables high capacity and cycling stability.[14, 46-49]

Figure 2 shows the 1st and 2nd cycle charge/discharge profiles at a C-rate of C/10 and subsequent five cycles at 1C, for the three commercial $LiFePO_4$/C materials (LFP/C-1, LFP/C-2 and LFP/C-3) cycled against the corresponding $Li_{0.25}FePO_4$/C counter-and-reference electrodes, in the three artificial brines and the benchmark 0.5 M Li_2SO_4 aqueous solution. All batteries cycled in the benchmark Li_2SO_4 aqueous solution show performance comparable to that obtained in the organic electrolyte (Fig. S3), whereas much lower capacities were obtained in the brines. We note that higher lithium sequestration and release capacities have been reported for LFP/C-3 in brines in our previous work, [14] which we ascribe to small differences in the method of electrode preparation or manual cell assembly.

In our previous work, we observed that the capacities of $LiFePO_4$ materials for lithium sequestration and release (which correspond to the charge and discharge capacities, respectively, of the $LiFePO_4$ electrode cycled against $Li_{0.25}FePO_4$) were affected by the lithium-ion concentration and viscosity of the brines.[14] This is consistent with the fact that the capacities in the benchmark 0.5 M Li_2SO_4 solution are higher than in the brines, due to the much higher lithium ion concentration and low viscosity of the former (Table 2). And this is also consistent with the fact that the capacities in the 'Central Altiplano' brine, which has very low lithium concentration and high viscosity (Table 2), are much lower than in the other brines. Fortunately, as we will show below, these poor capacity issues are overcome when using core-shell $LiFePO_4$/C materials. Furthermore, issues of irreproducibility in the electrochemical measurements in brines, also noted in our previous work,[14] are also overcome with the use of the here developed core-shell $LiFePO_4$/C materials.

In order to elucidate the fundamental cause of the poor performance, we estimated the diffusion-limited C-rate in the different brines, as reported in the supporting information. The results of the calculations suggest that the capacities should not be limited by the rate of lithium-ion diffusion for C-rates lower than 0.7C for the Atacama and Central Altiplano brines and 2C for the Olaroz brine. However, poor wetting of the electrodes in the highly viscous brines would hinder lithium-ion transport further, thus enhancing diffusional limitations beyond our calculations. On the other hand, high viscosity can also produce sluggish electron transfer reactions,[50] and thus, the identification of the rate determining step is currently unclear. In contrast to the commercial materials, the novel core-shell $LiFePO_4$/C materials here employed have small and homogenous particle size, without particle agglomerates, which facilitates fast mass transport, due to low tortuosity, as well as fast electron transfer, due to the small particle size. Indeed, as we will show below, the performance for lithium production applications is far superior to that of the commercial materials.

For the best performing commercial $LiFePO_4$/C material, LFP/C-3, additional experiments were undertaken to evaluate the long-term stability during the electrochemical cycling in brines. Figure 3 shows the 1st, 2nd and 50th cycle charge/discharge plots and the cycling stability, at a C-rate of C/10 in the artificial brines (Atacama, Olaroz and Central Altiplano) and the benchmark 0.5 M Li_2SO_4 solution. In all cases, the capacity of the brines is inferior to that obtained in the benchmark Li_2SO_4 solution, where the capacity in the latter starts with a value of ca. 155 mA h g^{-1} and drops to ca. 130 mA h g^{-1} after 50 cycles. The capacities in the Atacama and Olaroz brines are, initially, close to 100 mA h g^{-1}, then rapidly increase to ca. 140 mA h g^{-1} in the first few cycles, and then gradually decrease to 130-125 mA h g^{-1} after 50 cycles. Finally, the capacities in the Central Altiplano brine show a slow, steady increase from

ca. 20 mA h g^{-1} to 115 mA h g^{-1} after 50 cycles. Importantly, all these capacity values are inferior to what is obtained with the core-shell $LiFePO_4$/C material, as shown below.

3.3. Characterisation of core-shell $LiFePO_4$/C materials

Three kinds of nanosized core-shell structured $LiFePO_4$/C samples (LFP/C-4, LFP/C-5 and LFP/C-6) were prepared via a solvothermal synthesis method that enables an outstanding control in the particle size and quality of the carbon coating. The crystallite and particle sizes, carbon contents and coverages of $LiFePO_4$/C samples are summarised in Table 1. Contrary to the commercial materials, these core-shell materials exhibit crystallite and particle sizes that are in very good agreement (where the latter are slightly bigger, as expected, due to the carbon coating). The agreement in crystallite and particle sizes evidences that the $LiFePO_4$ crystalline grains do not agglomerate forming larger particles, which is highly advantageous to produce $LiFePO_4$/C electrodes with low tortuosity. The full and homogenous carbon coating of the core-shell materials is also highly advantageous, and here, the solvothermal synthesis method has been adapted to produce a range in the carbon content values to investigate the optimal carbon content for lithium production applications, as described below in detail.

The crystal structure properties of the core-shell $LiFePO_4$/C materials were studied by XRD, and the results are shown in Figure 4a. As for the commercial materials, all the XRD peaks of $LiFePO_4$/C samples can be indexed to the standard olivine $LiFePO_4$ structure. Fig. S4 shows the Rietveld fits to the XRD patterns, and the obtained lattice parameters (*a*, *b* and *c*), crystallite size broadening term (L_x) and reliability factors (R_{wp}, R_p) are listed in Table S3. These crystal structure properties are fully consistent with the values obtained for the commercial $LiFePO_4$/C materials, listed in Table S2. The crystallite sizes (Table 1) are the same, within the experimental uncertainty, for the three core-shell $LiFePO_4$/C materials

(123±7 nm), and slightly smaller than in the commercial samples (178±13 nm). The particle size distribution has been obtained from the analysis of the SEM images (Figure 4c), and all core-shell materials show a narrow size distribution with a consistent value of the average particle size, within the experimental uncertainty, of ~141±11 nm (Table 1). The particle sizes are much more homogeneous than in the commercial samples and, on average, also smaller (Table 1, Figure 1c), which will be shown below to be advantageous in lithium production applications.

The carbon contents of the core-shell $LiFePO_4$/C samples were estimated by TGA (Figure 4b), providing carbon content values of 2.2 wt%, 5.1 wt% and 8.0 wt% for LFP/C-4, LFP/C-5 and LFP/C-6, respectively, as listed in Table 1. The TEM images of samples (Figure 4d) show that the carbon layer has a thickness of ~5 nm and it is fully and evenly coated on the surface of the $LiFePO_4$ particles, thus confirming the core-shell structure of the $LiFePO_4$/C nanocomposites with a $LiFePO_4$-core covered by a carbon-shell.

For the electrochemical testing of the core-shell $LiFePO_4$/C materials for lithium production applications, it is necessary to produce the delithatiated $FePO_4$/C materials for the preparation of the counter-and-reference electrode. This was achieved by chemical delithiation, as explained in the Experimental methods section. The carbon content and coverages of the thus obtained $FePO_4$/C materials are summarised in Table S1. The results of the XRD characterisation (Fig. S5a) show the expected heterosite structure, as with the commercial samples. The SEM images (Fig. S5c) show that the particle morphology is not affected by the chemical delithiation process. The carbon content was estimated by TGA (Fig. S5b), providing carbon content values of 2.3 wt%, 5.2 wt% and 8.3 wt% for FP/C-4, FP/C-5 and FP/C-6, respectively (Table S1), in good agreement with the results of the parent lithiated materials (Table 1). The TEM images (Fig. S5d) show that the carbon layer is full and evenly

coated on the surface of the $FePO_4$ particles, which confirm that the carbon coating is not affected by the chemical delithiation process.

3.4. Electrochemical performance of core-shell $LiFePO_4$/C materials

The electrochemical properties of the core-shell $LiFePO_4$ materials (LFP/C-4, LFP/C-5 and LFP/C-6) were first assessed in lithium half-cells with an organic battery electrolyte (LP57), and the results (Fig. S6) are fully consistent with those obtained with the commercial materials (Fig. S3). Then, the electrochemical properties towards lithium sequestration and release in brines were evaluated using a $Li_{0.25}FePO_4$ counter-and-reference electrode, where the latter was prepared using a mixture of the lithiated, LFP/C, and delithiated, FP/C, of the same core-shell material produced via solvothermal synthesis. As shown in Figure 5, all the core-shell materials deliver high-capacity values for lithium sequestration and release in the brines and in the benchmark 0.5 M Li_2SO_4 aqueous solution. For LFP/C-4 and LFP/C-5, capacities of ca. 155-160 mA h g^{-1} were obtained at a C-rate of C/10, and only a moderate drop of capacity, to ca. 125-130 mA h g^{-1}, was observed when the C-rate increased to 1C. These capacity values correspond to high lithium sequestration amounts of 42-43 and 34-35 mg of lithium per gram of $FePO_4$, which is superior to previous reports.[24, 30, 51-53] For LFP/C-6, slightly smaller capacity values were obtained, possibly because of the thicker carbon coating in this sample (8.0 wt%),[54-56] but the performance is still much superior to that of the commercial materials (Figure 5). The improved performance of the core-shell $LiFePO_4$/C materials is ascribed to the homogeneity in particle size, which then produces low tortuosity electrodes where the transport of lithium ions is fast.[57-60] In addition, nanosizing of the core-shell $LiFePO_4$/C materials is also likely to contribute towards achieving high capacities, due to the increased surface area and the smaller diffusion pathlength.[61-63]

For the best performing core-shell $LiFePO_4$/C materials, the long-term cycling stability was evaluated with 50 cycles of lithium sequestration and release in the brines and in the benchmark 0.5 M Li_2SO_4 solution, at a C-rate of C/10 (Figure 6 and Fig. S7). Regardless the electrolyte composition, the capacity after 50 cycles was close to 135-140 mA h g^{-1}, corresponding to >87% capacity retention. In comparison, a capacity of only 30 mA h g^{-1}, with 21% capacity retention, was obtained after 25 cycles at 1C in a study by Trocoli et al.[23] Lithium absorption corresponding to a capacity of 104 mA h g^{-1}, with 84 % capacity retention, was reported after 50 cycles at 0.3 mA cm^{-2} by He et al.[24] A capacity of 41 mA h g^{-1}, with 85% capacity retention, were obtained after 100 cycles at 0.1 A g^{-1} by Wang et al.[30] Finally, capacities of 126 to 144 mA h g^{-1}, with capacity retention of 79% to 90%, were obtained after 50 cycles at C/10 in our previous study.[14] It is clear that the present core-shell $LiFePO_4$/C materials lead to higher long-term cycling capacities, which is attributed to two main factors: i) the full coverage of the carbon coating on the $LiFePO_4$ particles, which prevents interfacial degradation reactions that would otherwise occur when the $LiFePO_4$ material is in direct contact with the brines,[30, 47, 64-69] and ii) the nanosizing and homogeneity in particle size of the core-shell $LiFePO_4$/C materials, which prevents particle cracking and thus ensures that the homogeneous particle size is retained during cycling, hence also retaining the low electrode tortuosity associated with the homogeneous particle size.

Particle cracking has been suggested as the main cause for capacity degradation of $LiFePO_4$ for applications into lithium production from brines.[14] Interestingly, $LiFePO_4$ particle cracking has also been suggested to be the main cause of degradation of graphite-$LiFePO_4$ batteries, where it was shown that larger $LiFePO_4$ undergo more severe cracking, thus leading to faster degradation (due to a faster rate of lithium inventory loss).[70] The controlled nanosizing of the $LiFePO_4$ particles achieved with the present solvothermal synthesis method is, thus, critical to prevent particle cracking and the associated degradation. On the other hand,

while full carbon coverage on the $LiFePO_4$ particles is not needed for battery applications with organic electrolytes,[61, 71] for the present application of lithium production, the carbon coating acts as a protective layer to prevent degradation.

To investigate the causes of capacity degradation during cycling of the $LiFePO_4$ materials in brines, the electrodes were extracted from the cells after 50 cycles of lithium sequestration and release at C/10, and were characterised by XRD, Raman and SEM. Figure 7 shows the results of the characterisation of the $LiFePO_4$ working electrodes and Fig. S8 shows those for the $Li_{0.25}FePO_4$ counter-and-reference electrodes. As expected, the XRD patterns agree well with olivine $LiFePO_4$ and heterosite $FePO_4$ structures, and the Raman spectra show the characteristic D and G bands of amorphous carbon.[72-74] In both cases, minimal changes on the XRD and Raman signatures are observed during cycling, which indicates that minimal changes in the crystallographic structure of the $LiFePO_4$ and $FePO_4$ materials, nor on the carbon coating, have been induced during cycling. The SEM characterisation of the electrodes does not show any visible signs of particle cracking, in agreement with the high-capacity retention achieved with the present core-shell $LiFePO_4$/C materials.

4. Conclusion

Here we show that the commercial, carbon-coated $LiFePO_4$ materials, designed for non-aqueous lithium-ion batteries, are not appropriate for applications in the production of lithium from brines. By using a solvothermal synthesis method, we have prepared core-shell nanostructured $LiFePO_4$/C materials with a $LiFePO_4$-core (~123 nm size) fully covered by a thin carbon coating (~5 nm thickness), which significantly outperform the three types of $LiFePO_4$/C commercial materials here studied. While the commercial materials exhibit low capacity and stability issues, the optimised core-shell materials exhibit high capacities of up to 160 mA h g^{-1} and 130 mA h g^{-1} at C-rates of C/10 and 1C, respectively, and >87% capacity

retention after 50 cycles of lithium sequestration and release at C/10, for all the brine compositions studied. Due to the unavoidable changes in composition of natural brine resources, the observed consistency in performance regardless the brine composition is a bit asset.

The improved performance of the core-shell material is ascribed to the narrow particle size distribution, achieved by the controlled growth of particles in the solvothermal synthesis method. As a result, the battery electrodes made with the core-shell materials exhibit low tortuosity for the pathways of lithium-ion transport inside the brine-filled electrode pores, which thus produces a fast lithium-ion supply for the lithium sequestration reactions, leading to high capacities. Moreover, the present solvothermal synthesis method produces nanosized $LiFePO_4$/C, thus enabling fast reaction kinetics and preventing the issues of particle cracking associated with larger particles. Without particle cracking, the homogeneous particle size is preserved over cycling, and the protective carbon coating is also well-maintained, thus avoiding the surface degradation reactions that occur when the bare $LiFePO_4$ is in direct contact with the brines.

We hope that this work will inspire further studies to test these materials in flow reactors representative of commercial lithium production applications, where factors beyond those considered here (e.g. drastic concentration gradients, high temperature, impurities, open air conditions, etc.) bring additional challenges in materials design.

Conflicts of interest

There are no conflicts to declare.

Acknowledgements

Profs. Philip Bartlett, Andrew L. Hector, Ernesto Calvo and Victoria Flexer are gratefully acknowledged for fruitful scientific discussions. The authors also thank the Royal Society for support under the project "A highly versatile selective approach for lithium production" (IC170232). The authors also thank Patricia Goggin, Nikolay Zhelev, Regan Doherty and James Thompson for help in the TEM and SEM; and thank Andrea Russell for access to the Raman spectrometers. NGA thanks the EPSRC for an early career fellowship (EP/N024303/1). The data for this article are available from the University of Southampton at https://doi.org/10.5258/SOTON/D2684.

References

[1] J.W. Choi, D. Aurbach, Promise and reality of post-lithium-ion batteries with high energy densities, Nat. Rev. Mater., 1 (2016) 1-16.
[2] M. Li, J. Lu, Z. Chen, K. Amine, 30 years of lithium-ion batteries, Adv. Mater., 30 (2018) 1800561.
[3] R. Schmuch, R. Wagner, G. Hörpel, T. Placke, M. Winter, Performance and cost of materials for lithium-based rechargeable automotive batteries, Nat. Energy, 3 (2018) 267-278.
[4] A. Battistel, M.S. Palagonia, D. Brogioli, F. La Mantia, R. Trocoli, Electrochemical methods for lithium recovery: A comprehensive and critical review, Adv. Mater., 32 (2020) 1905440.
[5] V. Flexer, C.F. Baspineiro, C.I. Galli, Lithium recovery from brines: A vital raw material for green energies with a potential environmental impact in its mining and processing, Sci. Total Environ., 639 (2018) 1188-1204.
[6] H. Vikström, S. Davidsson, M. Höök, Lithium availability and future production outlooks, Appl. Energy, 110 (2013) 252-266.
[7] C. Grosjean, P.H. Miranda, M. Perrin, P. Poggi, Assessment of world lithium resources and consequences of their geographic distribution on the expected development of the electric vehicle industry, Renew. Sustain. Energy Rev., 16 (2012) 1735-1744.
[8] K. Schulz, R. Seal, D. Bradley, J. Deyoung, Critical Mineral Resources of the United States-Economic and Environmental Geology and Prospects for Future Supply, U.S. Geological Survey, Reston, VA, USA, 2017.
[9] L. Talens Peiró, G. Villalba Méndez, R.U. Ayres, Lithium: sources, production, uses, and recovery outlook, Jom, 65 (2013) 986-996.
[10] S. Pérez-Rodríguez, J.A. Milton, N. Garcia-Araez, Novel method of lithium production from brines combining a battery material and sodium sulfite as a cheap and environmentally friendly reducing agent, ACS Sustain. Chem. Eng., 8 (2020) 6243-6251.
[11] G. Liu, Z. Zhao, A. Ghahreman, Novel approaches for lithium extraction from salt-lake brines: A review, Hydrometallurgy, 187 (2019) 81-100.
[12] B. Swain, Recovery and recycling of lithium: A review, Sep. Purif. Technol., 172 (2017) 388-403.
[13] Y. Sun, Q. Wang, Y. Wang, R. Yun, X. Xiang, Recent advances in magnesium/lithium separation and lithium extraction technologies from salt lake brine, Sep. Purif. Technol., 256 (2021) 117807.

[14] S. Perez-Rodriguez, S.D.S. Fitch, P.N. Bartlett, N. Garcia-Araez, LiFePO4 battery material for the production of lithium from brines: Effect of brine composition and benefits of dilution, ChemSusChem, 15 (2022) e202102182.
[15] N. Intaranont, N. Garcia-Araez, A.L. Hector, J.A. Milton, J.R. Owen, Selective lithium extraction from brines by chemical reaction with battery materials, J. Mater. Chem. A, 2 (2014) 6374-6377.
[16] M. Pasta, A. Battistel, F. La Mantia, Batteries for lithium recovery from brines, Energy Environ. Sci., 5 (2012) 9487-9491.
[17] J. Lee, S.H. Yu, C. Kim, Y.E. Sung, J. Yoon, Highly selective lithium recovery from brine using a lambda-MnO2-Ag battery, Phys. Chem. Chem. Phys., 15 (2013) 7690-7695.
[18] R. Trocoli, A. Battistel, F.L. Mantia, Selectivity of a lithium-recovery process based on LiFePO4, Chemistry, 20 (2014) 9888-9891.
[19] R. Trocoli, A. Battistel, F. La Mantia, Nickel hexacyanoferrate as suitable alternative to Ag for electrochemical lithium recovery, ChemSusChem, 8 (2015) 2514-2519.
[20] S. Kim, J. Lee, J.S. Kang, K. Jo, S. Kim, Y.E. Sung, J. Yoon, Lithium recovery from brine using a lambda-MnO2/activated carbon hybrid supercapacitor system, Chemosphere, 125 (2015) 50-56.
[21] J.S. Kim, Y.H. Lee, S. Choi, J. Shin, H.C. Dinh, J.W. Choi, An electrochemical cell for selective lithium capture from seawater, Environ. Sci. Technol., 49 (2015) 9415-9422.
[22] L.L. Missoni, F. Marchini, M. del Pozo, E.J. Calvo, A LiMn2O4-polypyrrole system for the extraction of LiCl from natural brine, J. Electrochem. Soc., 163 (2016) A1898-A1902.
[23] R. Trócoli, C. Erinmwingbovo, F. La Mantia, Optimized lithium recovery from brines by using an electrochemical ion-pumping process based on λ-MnO2 and nickel hexacyanoferrate, ChemElectroChem, 4 (2017) 143-149.
[24] L. He, W. Xu, Y. Song, Y. Luo, X. Liu, Z. Zhao, New insights into the application of lithium-ion battery materials: selective extraction of lithium from brines via a rocking-chair lithium-ion battery system, Glob. Chall., 2 (2018) 1700079.
[25] M.S. Palagonia, D. Brogioli, F.L. Mantia, Influence of hydrodynamics on the lithium recovery efficiency in an electrochemical ion pumping separation process, J. Electrochem. Soc., 164 (2017) E586-E595.
[26] E.J. Calvo, Electrochemical methods for sustainable recovery of lithium from natural brines and battery recycling, Curr. Opin. Electrochem., 15 (2019) 102-108.
[27] F. Marchini, F.J. Williams, E.J. Calvo, Sustainable selective extraction of lithium chloride from natural brine using a Li1-xMn2O4 ion pump, J. Electrochem. Soc., 165 (2018) A3292-A3298.
[28] S. Kim, J.S. Kang, H. Joo, Y.E. Sung, J. Yoon, Understanding the behaviors of lambda-MnO2 in electrochemical lithium recovery: key limiting factors and a route to the enhanced performance, Environ. Sci. Technol., 54 (2020) 9044-9051.
[29] N. Xie, Y. Li, Y. Lu, J. Gong, X. Hu, Electrochemically controlled reversible lithium capture and release enabled by LiMn2O4 nanorods, ChemElectroChem, 7 (2020) 105-111.
[30] L. Wang, K. Frisella, P. Srimuk, O. Janka, G. Kickelbick, V. Presser, Electrochemical lithium recovery with lithium iron phosphate: What causes performance degradation and how can we improve the stability?, Sustain. Energy Fuels, 5 (2021) 3124-3133.
[31] Y. Liu, M. Zhang, Y. Li, Y. Hu, M. Zhu, H. Jin, W. Li, Nano-sized LiFePO4/C composite with core-shell structure as cathode material for lithium ion battery, Electrochim. Acta, 176 (2015) 689-693.
[32] C.V. Ramana, A. Mauger, F. Gendron, C.M. Julien, K. Zaghib, Study of the Li-insertion/extraction process in LiFePO4/FePO4, J. Power Sources, 187 (2009) 555-564.
[33] A. Larson, R. Von Dreele, L. Finger, M. Kroeker, B. Toby, Lecture goal, J. Appl. Crystallogr., 34 (2001) 210-213.
[34] F. Marchini, E.J. Calvo, F.J. Williams, Effect of the electrode potential on the surface composition and crystal structure of LiMn2O4 in aqueous solutions, Electrochim. Acta, 269 (2018) 706-713.
[35] F. Risacher, B. Fritz, Quaternary geochemical evolution of the salars of Uyuni and Coipasa, Central Altiplano, Bolivia, Chem. Geol., 90 (1991) 211-231.
[36] M.L. Vera, W.R. Torres, C.I. Galli, A. Chagnes, V. Flexer, Environmental impact of direct lithium extraction from brines, Nat. Rev. Earth Environ., 4 (2023) 149-165.

[37] J.W. An, D.J. Kang, K.T. Tran, M.J. Kim, T. Lim, T. Tran, Recovery of lithium from Uyuni salar brine, Hydrometallurgy, 117 (2012) 64-70.
[38] D.E. Garrett, Handbook of Lithium and Natural Calcium Chloride, Academic Press, California, USA, 2004.
[39] R. Thomas, Titanium in the geothermal industry, Geothermics, 32 (2003) 679-687.
[40] N. Ryall, N. Garcia-Araez, Highly sensitive operando pressure measurements of Li-ion battery materials with a simply modified Swagelok cell, J. Electrochem. Soc., 167 (2020) 110511.
[41] M. Zhang, N. Garcia-Araez, A.L. Hector, J.R. Owen, R.G. Palgrave, M.G. Palmer, S. Soulé, Solvothermal water-diethylene glycol synthesis of LiCoPO4 and effects of surface treatments on lithium battery performance, RSC Adv., 9 (2019) 740-752.
[42] M. Zhang, N. Garcia-Araez, A.L. Hector, J.R. Owen, A sol–gel route to titanium nitride conductive coatings on battery materials and performance of TiN-coated LiFePO4, J. Mater. Chem. A, 5 (2017) 2251-2260.
[43] A.K. Padhi, K.S. Nanjundaswamy, J.B. Goodenough, Phospho-olivines as positive-electrode materials for rechargeable lithium batteries, J. Electrochem. Soc., 144 (1997) 1188-1194.
[44] C.-H. Yim, E.A. Baranova, Y. Abu-Lebdeh, I. Davidson, Highly ordered LiFePO4 cathode material for Li-ion batteries templated by surfactant-modified polystyrene colloidal crystals, J. Power Sources, 205 (2012) 414-419.
[45] I. Belharouak, C. Johnson, K. Amine, Synthesis and electrochemical analysis of vapor-deposited carbon-coated LiFePO4, Electrochem. Commun., 7 (2005) 983-988.
[46] P. He, X. Zhang, Y.-G. Wang, L. Cheng, Y.-Y. Xia, Lithium-ion intercalation behavior of LiFePO4 in aqueous and nonaqueous electrolyte solutions, J. Electrochem. Soc., 155 (2007) A144-A150.
[47] P. He, J.-L. Liu, W.-J. Cui, J.-Y. Luo, Y.-Y. Xia, Investigation on capacity fading of LiFePO4 in aqueous electrolyte, Electrochim. Acta, 56 (2011) 2351-2357.
[48] D. Gordon, M.Y. Wu, A. Ramanujapuram, J. Benson, J.T. Lee, A. Magasinski, N. Nitta, C. Huang, G. Yushin, Enhancing cycle stability of lithium iron phosphate in aqueous electrolytes by increasing electrolyte molarity, Adv. Energy Mater., 6 (2016) 1501805.
[49] X. Zeng, Q. Liu, M. Chen, L. Leng, T. Shu, L. Du, H. Song, S. Liao, Electrochemical Behavior of Spherical LiFePO4/C Nanomaterial in Aqueous Electrolyte, and Novel Aqueous Rechargeable Lithium Battery with LiFePO4/C anode, Electrochimica Acta, 177 (2015) 277-282.
[50] M.J. Weaver, Dynamical solvent effects on activated electron-transfer reactions: principles, pitfalls, and progress, Chem. Rev., 92 (1992) 463-480.
[51] Z. Zhao, X. Si, X. Liu, L. He, X. Liang, Li extraction from high Mg/Li ratio brine with LiFePO4/FePO4 as electrode materials, Hydrometallurgy, 133 (2013) 75-83.
[52] X. Liu, X. Chen, Z. Zhao, X. Liang, Effect of Na+ on Li extraction from brine using LiFePO4/FePO4 electrodes, Hydrometallurgy, 146 (2014) 24-28.
[53] T. Han, X. Yu, Y. Guo, M. Li, J. Duo, T. Deng, Green recovery of low concentration of lithium from geothermal water by a novel FPO/KNiFC ion pump technique, Electrochim. Acta, 350 (2020) 136385.
[54] R. Dominko, M. Bele, M. Gaberscek, M. Remskar, D. Hanzel, S. Pejovnik, J. Jamnik, Impact of the carbon coating thickness on the electrochemical performance of LiFePO4/C composites, J. Electrochem. Soc., 152 (2005) A607-A610.
[55] M. Zhang, N. Garcia-Araez, A.L. Hector, Understanding and development of olivine LiCoPO4 cathode materials for lithium-ion batteries, J. Mater. Chem. A, 6 (2018) 14483-14517.
[56] J. Wang, X. Sun, Understanding and recent development of carbon coating on LiFePO4 cathode materials for lithium-ion batteries, Energy Environ. Sci., 5 (2012) 5163-5185.
[57] B. Vijayaraghavan, D.R. Ely, Y.-M. Chiang, R. García-García, R.E. García, An analytical method to determine tortuosity in rechargeable battery electrodes, J. Electrochem. Soc., 159 (2012) A548-A552.
[58] M. Ebner, D.-W. Chung, R.E. García, V. Wood, Tortuosity anisotropy in lithium-ion battery electrodes, Adv. Energy Mater., 4 (2014) 1301278.
[59] D. Kehrwald, P.R. Shearing, N.P. Brandon, P.K. Sinha, S.J. Harris, Local tortuosity inhomogeneities in a lithium battery composite electrode, J. Electrochem. Soc., 158 (2011) A1393-A1399.

[60] J. Landesfeind, M. Ebner, A. Eldiven, V. Wood, H.A. Gasteiger, Tortuosity of battery electrodes: validation of impedance-derived values and critical comparison with 3D tomography, J. Electrochem. Soc., 165 (2018) A469-A476.
[61] C. Delacourt, P. Poizot, S. Levasseur, C. Masquelier, Size effects on carbon-free LiFePO4 powders: The key to superior energy density, Electrochem. Solid-State Lett., 9 (2006) A352-A355.
[62] R. Malik, D. Burch, M. Bazant, G. Ceder, Particle size dependence of the ionic diffusivity, Nano Lett., 10 (2010) 4123-4127.
[63] F.C. Strobridge, B. Orvananos, M. Croft, H.-C. Yu, R. Robert, H. Liu, Z. Zhong, T. Connolley, M. Drakopoulos, K. Thornton, C.P. Grey, Mapping the inhomogeneous electrochemical reaction through porous LiFePO4-electrodes in a standard coin cell battery, Chem. Mater., 27 (2015) 2374-2386.
[64] Z. Li, K.C. Smith, Y. Dong, N. Baram, F.Y. Fan, J. Xie, P. Limthongkul, W.C. Carter, Y.M. Chiang, Aqueous semi-solid flow cell: demonstration and analysis, Phys. Chem. Chem. Phys., 15 (2013) 15833-15839.
[65] K. Zaghib, M. Dontigny, P. Charest, J.F. Labrecque, A. Guerfi, M. Kopec, A. Mauger, F. Gendron, C.M. Julien, Aging of LiFePO4 upon exposure to H2O, J. Power Sources, 185 (2008) 698-710.
[66] J.F. Martin, A. Yamada, G. Kobayashi, S.-i. Nishimura, R. Kanno, D. Guyomard, N. Dupré, Air exposure effect on LiFePO4, Electrochem. Solid-State Lett., 11 (2008) A12-A16.
[67] W. Porcher, P. Moreau, B. Lestriez, S. Jouanneau, D. Guyomard, Is LiFePO4 stable in water?: Toward greener Li-ion batteries, Electrochem. Solid-State Lett., 11 (2008) A4-A8.
[68] D.Y.W. Yu, K. Donoue, T. Kadohata, T. Murata, S. Matsuta, S. Fujitani, Impurities in LiFePO4 and their influence on material characteristics, J. Electrochem. Soc., 155 (2008) A526-A530.
[69] P. Byeon, H.B. Bae, H.-S. Chung, S.-G. Lee, J.-G. Kim, H.J. Lee, J.W. Choi, S.-Y. Chung, Atomic-scale observation of LiFePO4 and LiCoO2 dissolution behavior in aqueous solutions, Adv. Funct. Mater., 28 (2018) 1804564.
[70] E.R. Logan, A. Eldesoky, Y. Liu, M. Lei, X. Yang, H. Hebecker, A. Luscombe, M.B. Johnson, J.R. Dahn, The effect of LiFePO4 particle size and surface area on the performance of LiFePO4/graphite cells, J. Electrochem. Soc., 169 (2022) 050524.
[71] M. Gaberscek, R. Dominko, J. Jamnik, Is small particle size more important than carbon coating? An example study on LiFePO4 cathodes, Electrochem. Commun., 9 (2007) 2778-2783.
[72] A.C. Ferrari, J. Robertson, Interpretation of Raman spectra of disordered and amorphous carbon, Phys. Rev. B, 61 (2000) 14095-14107.
[73] A.C. Ferrari, J. Robertson, Resonant Raman spectroscopy of disordered, amorphous, and diamondlike carbon, Phys. Rev. B, 64 (2001) 075414.
[74] A.C. Ferrari, J. Robertson, Raman spectroscopy of amorphous, nanostructured, diamond-like carbon, and nanodiamond, Phil. Trans. R. Soc. Lond. A, 362 (2004) 2477-2512.

FIGURES

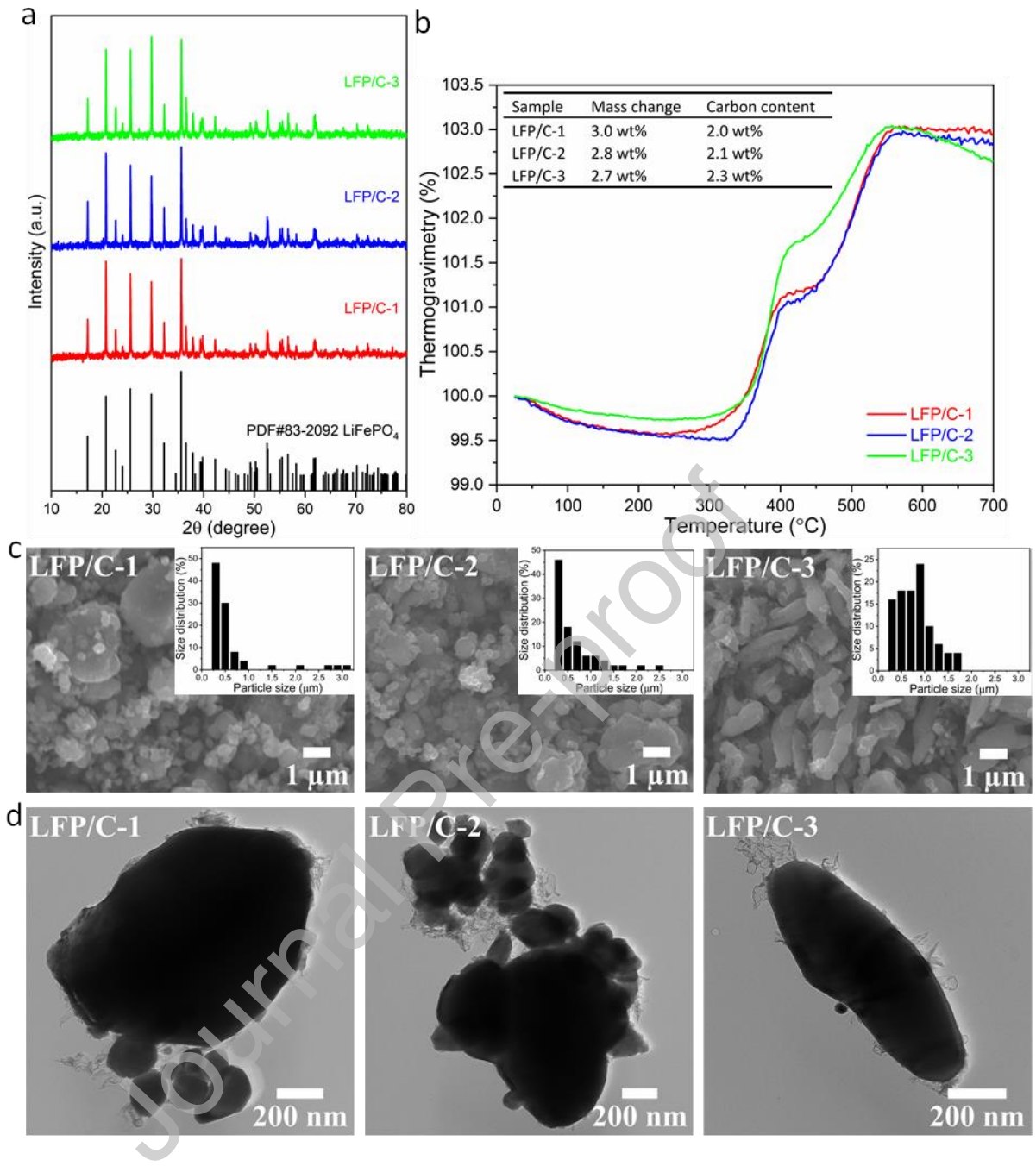
a
LFP/C-3
LFP/C-2
LFP/C-1
PDF#83-2092 LiFePO4
Intensity (a.u.)
2θ (degree)
b
Sample | Mass change | Carbon content
LFP/C-1 | 3.0 wt% | 2.0 wt%
LFP/C-2 | 2.8 wt% | 2.1 wt%
LFP/C-3 | 2.7 wt% | 2.3 wt%
Thermogravimetry (%)
Temperature (°C)
LFP/C-1
LFP/C-2
LFP/C-3
c
LFP/C-1
LFP/C-2
LFP/C-3
Size distribution (%)
Particle size (μm)
1 μm
d
LFP/C-1
LFP/C-2
LFP/C-3
200 nm

Figure 1

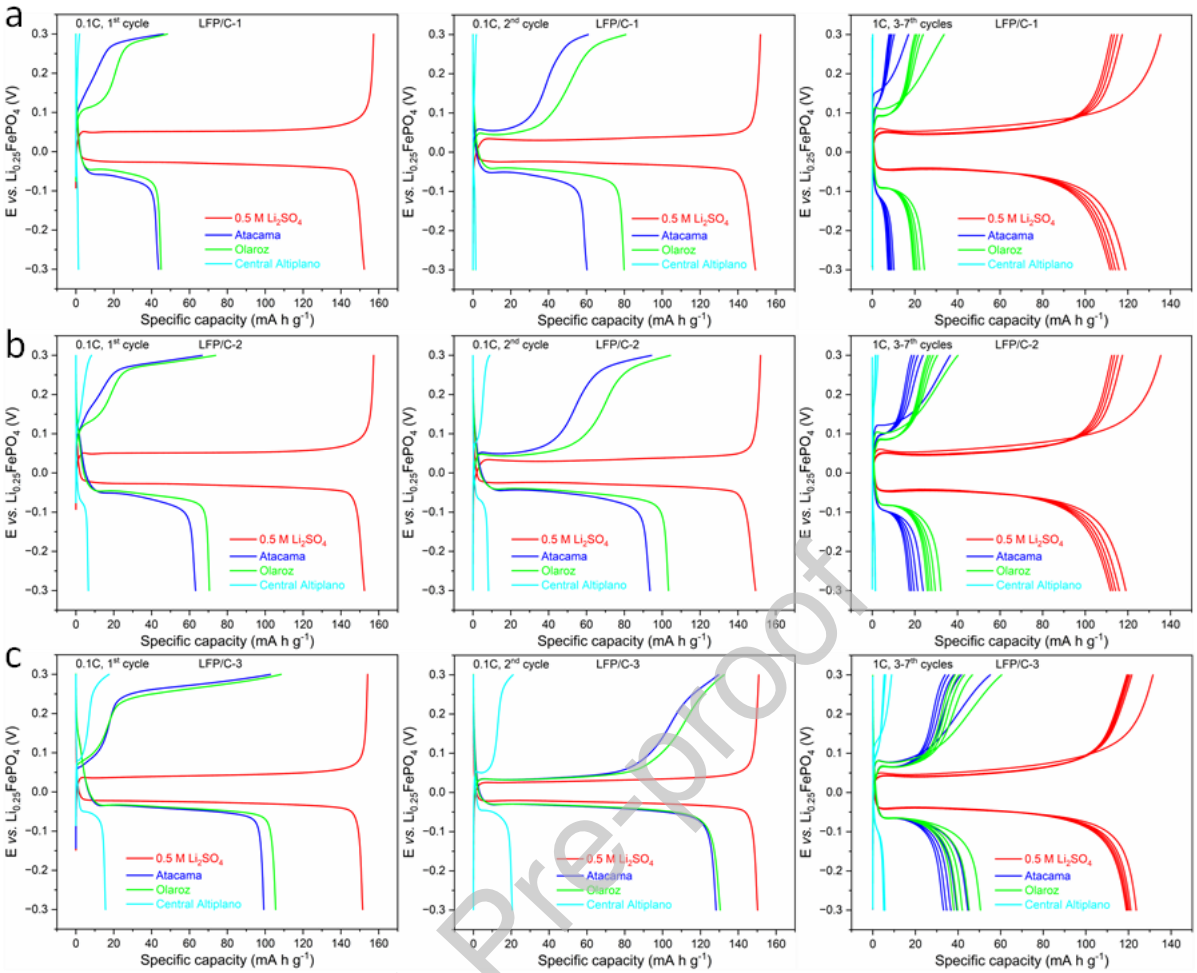

Figure 2

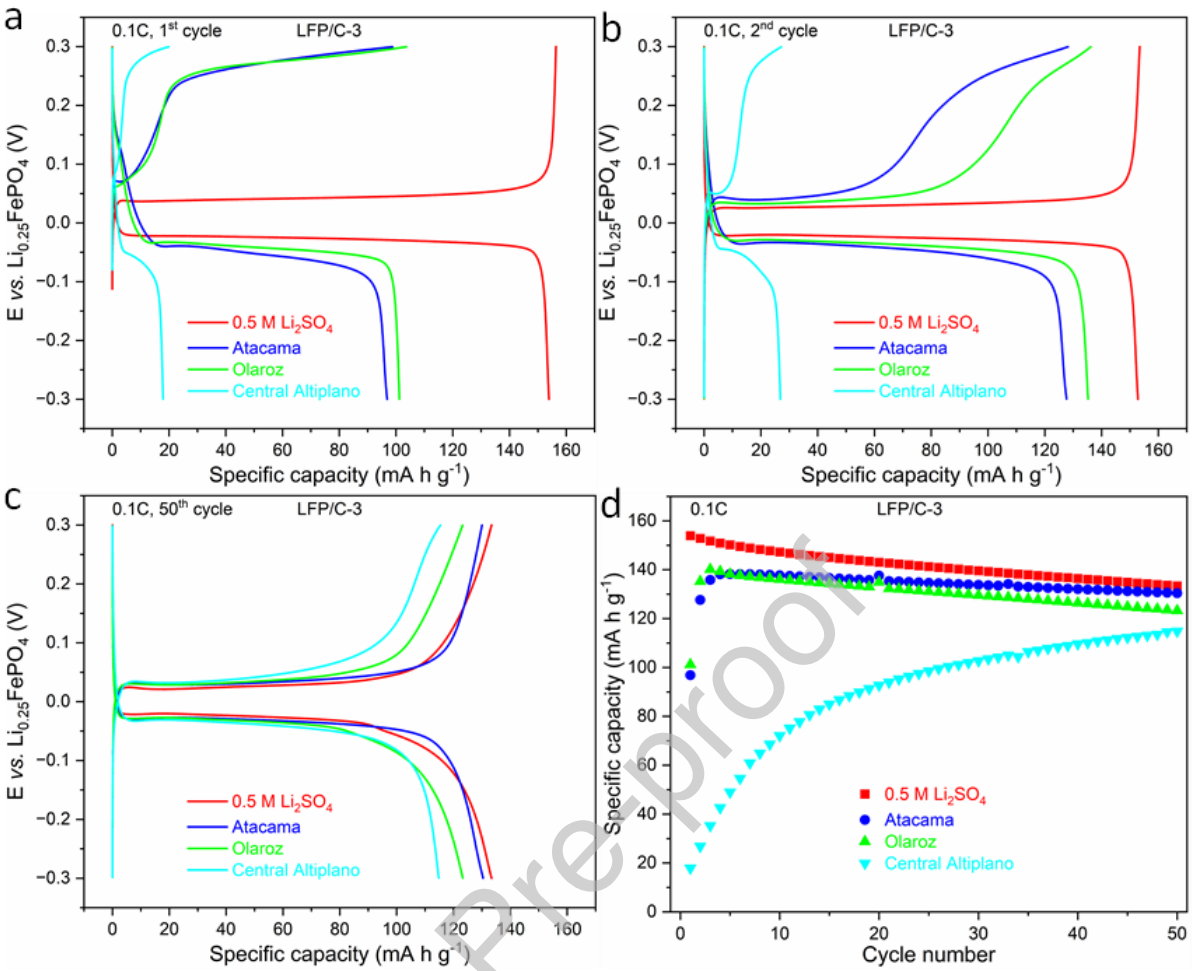

Figure 3

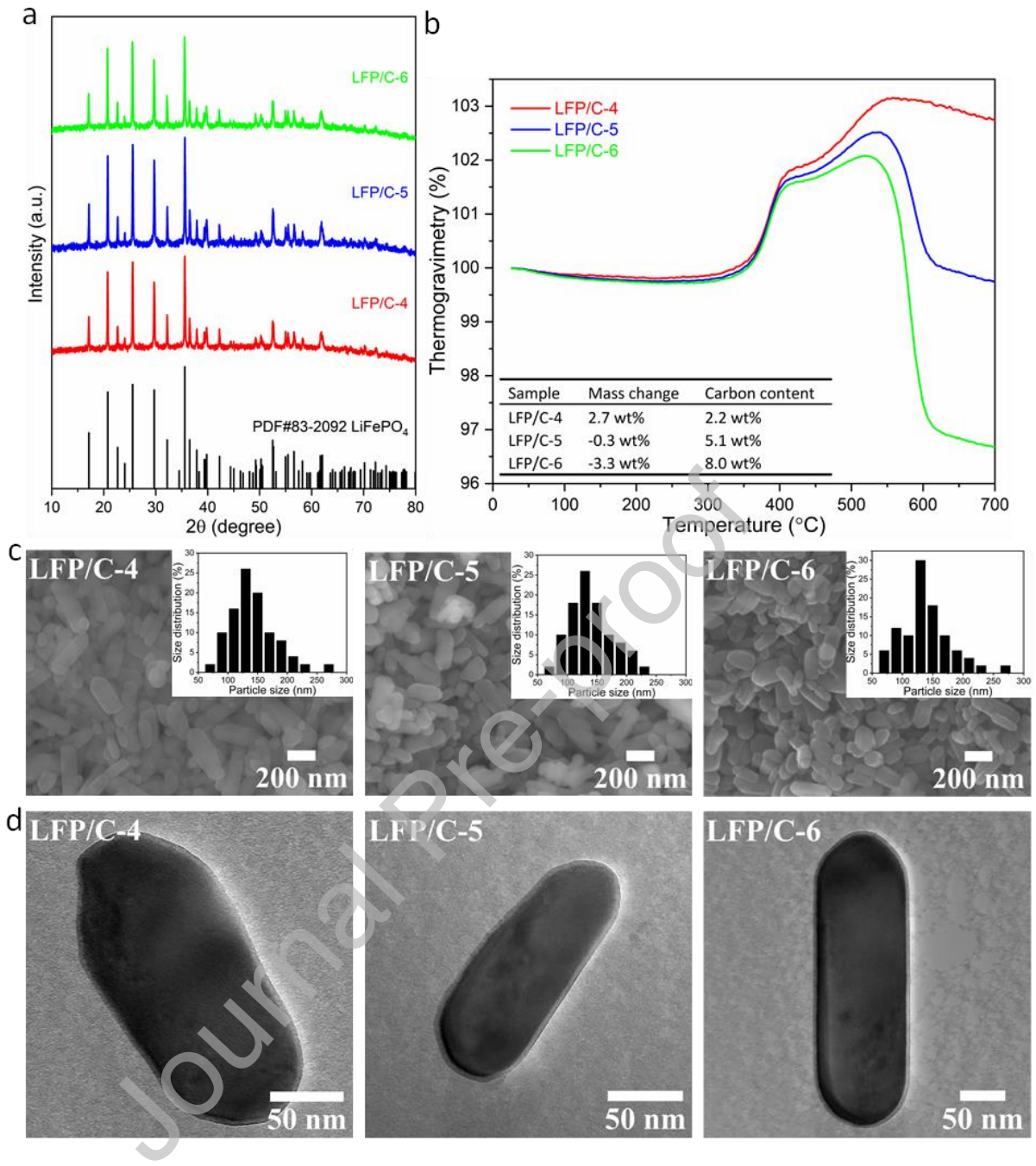

Figure 4

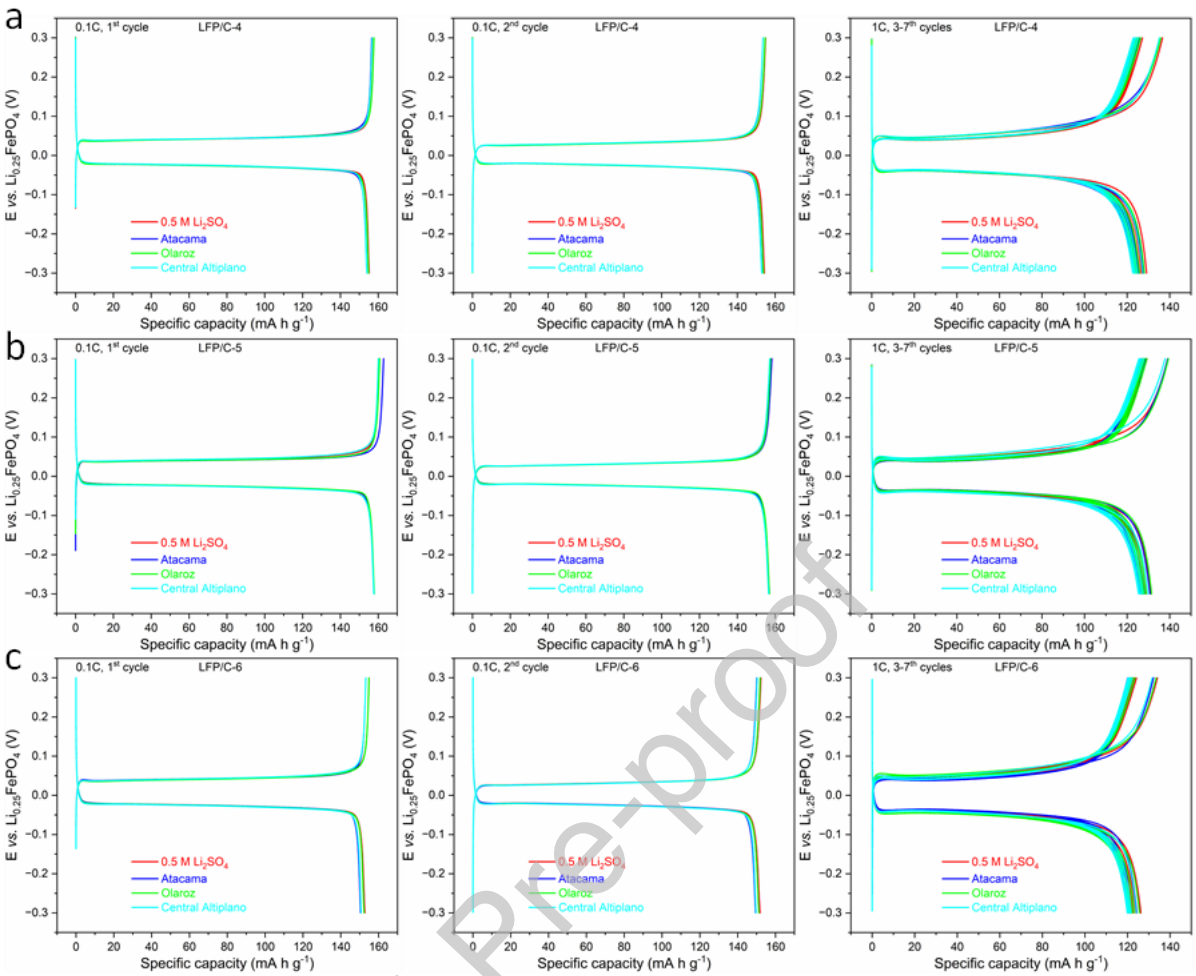

Figure 5

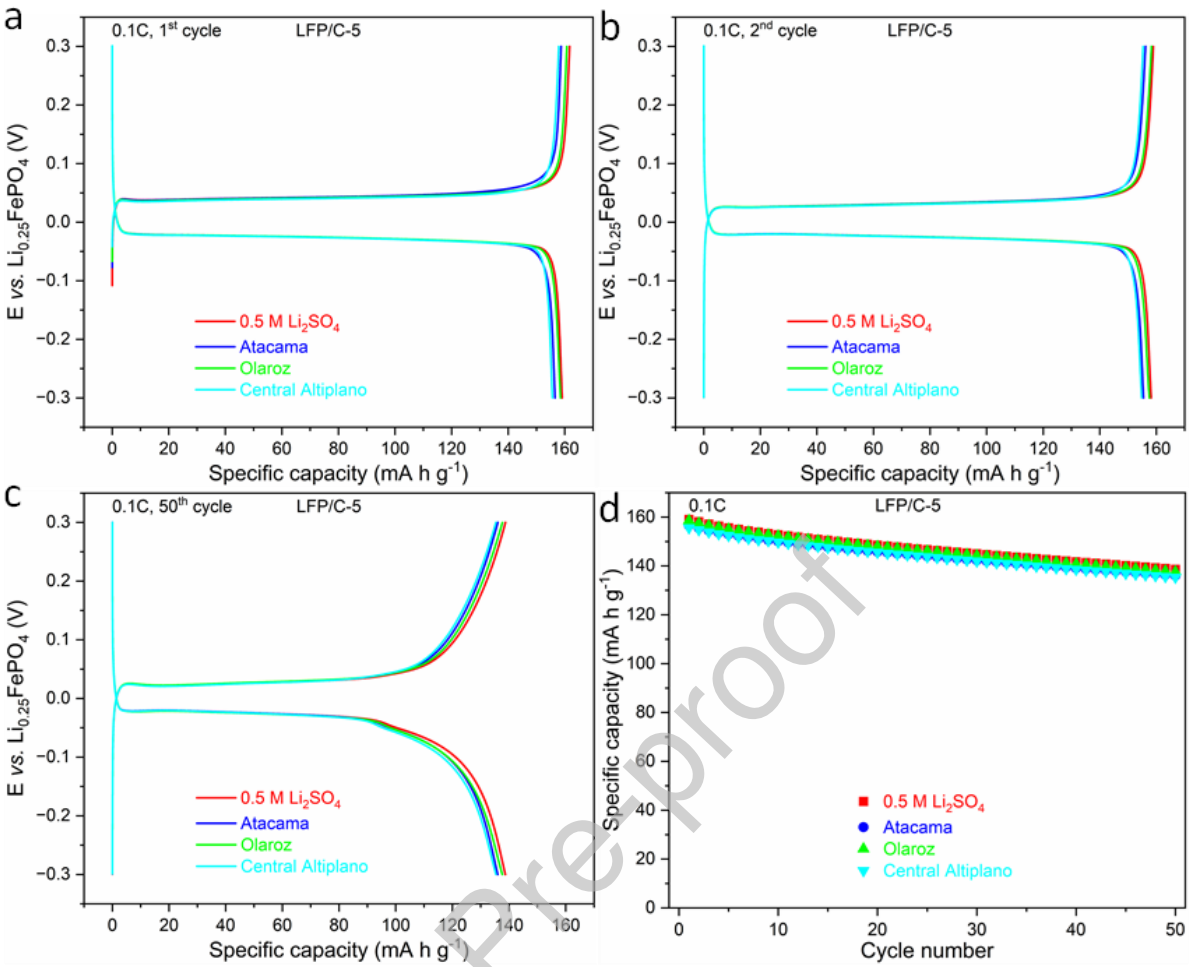

Figure 6

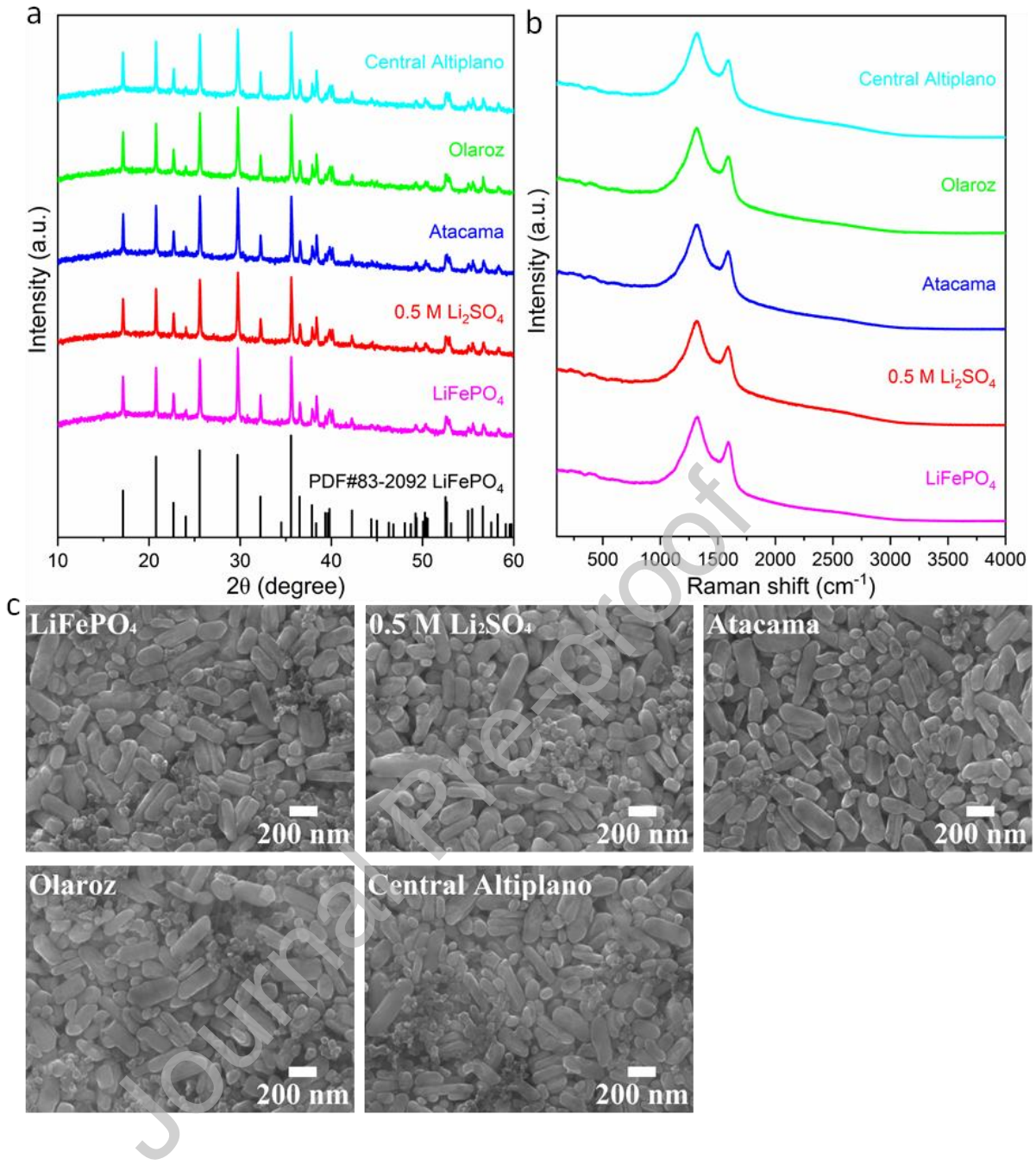

Figure 7

FIGURE CAPTIONS

Figure 1 (a) XRD patterns, (b) TGA analyses, (c) SEM images and (d) TEM images of LFP/C-1, LFP/C-2 and LFP/C-3 samples; the particle size determined by using the ImageJ software to analyse SEM images (sample labels explained in Table 1).

Figure 2 1st and 2nd cycle charge/discharge plots at a C-rate of C/10 and subsequent five cycles at 1C, for (a) LFP/C-1, (b) LFP/C-2 and (c) LFP/C-3 electrodes cycled against the corresponding $Li_{0.25}FePO_4$ counter-and-reference electrode in the artificial brines (Atacama, Olaroz and Central Altiplano) and the benchmark 0.5 M Li_2SO_4 solution (sample labels explained in Table 1).

Figure 3 (a) 1st, (b) 2nd and (c) 50th cycle charge/discharge plots at a C-rate of C/10 and (d) cycling stability, for LFP/C-3 electrodes cycled against the corresponding $Li_{0.25}FePO_4$ counter-and-reference electrode in the artificial brines (Atacama, Olaroz and Central Altiplano) and the benchmark 0.5 M Li_2SO_4 solution (sample labels explained in Table 1).

Figure 4 As in Figure 1 but for LFP/C-4, LFP/C-5 and LFP/C-6 samples (sample labels explained in Table 1).

Figure 5 As in Figure 2 but for (a) LFP/C-4, (b) LFP/C-5 and (c) LFP/C-6 samples (sample labels explained in Table 1).

Figure 6 As in Figure 3 but for the LFP/C-5 sample (sample labels explained in Table 1).

Figure 7 (a) XRD patterns, (b) Raman spectra and (c) SEM images of the pristine and cycled $LiFePO_4$ electrodes, where the latter were cycled for 50 cycles against $Li_{0.25}FePO_4$, at a C-rate of C/10, in the artificial brines (Atacama, Olaroz and Central Altiplano) and the benchmark 0.5 M Li_2SO_4 solution.

TABLES

Table 1 Properties of $LiFePO_4$/C samples: crystallite sizes obtained from Rietveld fits to XRD patterns; average particle sizes determined by using the ImageJ software to analyse

SEM images; carbon contents and coverages obtained through TGA analyses and TEM images, respectively.

Sample	Provider	Crystallite size (nm)	Average particle size (nm)	Carbon content (wt%)	Carbon coverage
LFP/C-1	MTI	180±13	630±190	2.0	
LFP/C-2	Li-FUN	181±13	620±140	2.1	Partial
LFP/C-3	Tatung	173±13	790±100	2.3	
LFP/C-4		124±7	142±11	2.2	
LFP/C-5	Self-made	120±7	142±10	5.1	Full
LFP/C-6		124±7	139±12	8.0	

Table 2 Molar concentrations of salts used to prepare artificial brines and the benchmark Li_2SO_4 solution. The values of the dynamic viscosity of the solutions are also included.[14]

Brine	LiCl (M)	NaCl (M)	KCl (M)	$MgCl_2$ (M)	Li_2SO_4 (M)	Viscosity (mPa s)
0.5 M Li_2SO_4	-	-	-	-	0.50	1.13
Atacama	0.04	0.78	0.10	0.07	-	0.97
Olaroz	0.18	5.00	0.28	-	-	1.79
Central Altiplano	0.06	4.00	0.20	0.30	-	1.60

Declaration of interests

☒The authors declare that they have no known competing financial interests or personal relationships that could have appeared to influence the work reported in this paper.

☐The authors declare the following financial interests/personal relationships which may be considered as potential competing interests:

Graphical abstract